Ozonolysis of diamond

Ozonolysis of diamond

Christian K Fink and Stephen J Jenkins

Department of Chemistry, University of Cambridge, Cambridge CB2 1EW, UK

Abstract

The oxidation of diamond is attracting increasing interest, in the light of efforts to modulate its electronic properties for device applications. Ozone is a promising candidate oxidant species, allowing low temperature processing compared with molecular dioxygen. Here, we present first-principles molecular dynamics simulations for the dissociative adsorption of ozone on the {001} surface of diamond, carried out at the level of density functional theory. We find that ozone readily oxidizes the surface, with two distinct modes of reaction: partial dissociation results in deposition of a single oxygen adatom in an alkoxide-like structure that rapidly converts to an epoxide-like configuration; complete dissociation results in two adatoms located in ketone-like structures, with a third occupying an alkoxide geometry, expected to revert to the epoxide in due course. We describe not only the structural changes during the reactions, but also the variations in electron and spin densities that reveal the bonding rearrangements.

(Some figures in this article are in colour only in the electronic version)

1. Introduction

Diamond exhibits unique mechanical, electronic and optical properties, which make it a promising material for future device technologies [1, 2]. In particular, diamond has a wide indirect band gap of 5.5 eV, resulting in excellent insulating properties. It exhibits a very high carrier mobility, for both holes and electrons, and the highest thermal conductivity of any material at room temperature. In terms of stability, diamond is not only resistant to radiation damage and chemically inert, but also biocompatible.

Taking advantage of these properties, diamond is already used in applications as wide-ranging as radiation detectors, chemical sensors, high-quality electrodes, and protective coatings for extreme conditions [3]. Nevertheless, to take advantage of diamond's full potential for electronic devices, it will be necessary to tune its electronic properties. Since dopants face difficulties in diffusing deep into the bulk material, surface modifications have been suggested as an alternative route to engineer the electronic properties [4]. For instance, by varying the coverage of certain adsorbates on the diamond surface, it is possible to tune its electron affinity and polarity. The most important terminations include hydrogen and oxygen, which result in opposite electronic and chemical surface properties.

Whereas oxygen termination leads to a hydrophilic surface and increases the electron affinity, hydrogen termination results in a hydrophobic surface and leads to a negative electron affinity; the latter is a highly unusual feature, and leads, in the presence of an electrolyte, to a highly conductive surface layer [5, 6]. This 'surface transfer doping' promises novel device applications [7]. Due to its opposite nature, the oxygen termination is routinely used to locally remove the high surface-conductivity of hydrogenated diamond.

Considerable theoretical and experimental research efforts have focused on the interaction between molecular oxygen (O_2) and diamond [8–12]. Despite its chemical inertness as a bulk material, the diamond surface was found to be fairly sensitive to oxygen exposure (i.e. diamond begins to oxidize in air at temperatures above around 400 °C). The most stable oxygen terminations on C{001} were found to be the ether (C–O–C) and ketone (>C=O) configurations. Yet, at temperatures above 800 °C, oxygen exposure leads to an extensive removal of surface carbon atoms ('etching') via the formation of gas-phase CO, which leaves shallow square etch pits on the surface [13, 14]. In contrast to the cases of other semiconducting materials (e.g. Si, Ge), O atoms are not able to diffuse into the subsurface, and therefore the oxidation of diamond saturates at the monolayer level.

Ozone (O_3) has already been used in a variety of applications as a more reactive oxidant of diamond. On hydrogen-passivated diamond surfaces, it was found that ozone has a positive effect on the surface-conductivity [15–17]. A theoretical investigation, studying the effect of a water adlayer on the hydrogen-terminated surface, attributed this behaviour to electron transfer from the surface into a chemisorbed O_3 species [18]. Moreover, Sakai *et al* [19] treated H-terminated polycrystalline diamond with

ozone to build a field-effect transistor, observing that ozone successfully oxidized the surface even at room temperature. Ozone has also been used to increase the cell adhesion forces in a biocompatibility study [20] and in the simultaneous purification and modification of detonation nanodiamonds [21].

Despite the growing body of experimental data, little is known about the microscopic oxidation mechanism of ozone on diamond. The most relevant study to date was carried out by Maranzana *et al* [22], who used density functional theory (DFT) to investigate the interaction of ozone with polycyclic aromatic hydrocarbons and graphene, which acted as a model for soot particles. The authors found that the oxidation exhibited a high activation barrier (e.g. their largest molecule, coronene, $C_{24}H_{12}$, yielded a barrier of 0.61 eV). In contrast, we will demonstrate below that the {001} diamond surface is much more reactive than these planar carbon structures.

2. Methodology

The results of all calculations presented here were obtained using DFT as implemented in CASTEP [23]. The approach uses Vanderbilt ultrasoft pseudopotentials [24] for electron–ion interactions and the Perdew–Wang generalized gradient approximation (GGA-PW91) for electron–electron interactions (exchange and correlation) [25], with a plane-wave basis set expanded to an energy cut-off at 340 eV to describe the electronic wavefunctions.

Integration over the Brillouin zone was carried out using a Monkhorst–Pack [26] mesh (MPM). The bulk lattice constant was determined to be $a = 3.539$ Å (exp: $a = 3.567$ Å [3]) and employed through fixed cell dimensions in all surface calculations. The {001} surface was modelled in a periodic supercell as a six-layer slab, with the bottom two layers fixed and the dangling bonds of the lowest layer passivated with hydrogen atoms. A vacuum region of 10 Å was found sufficient to prevent any interslab interactions[1]. A surface unit cell of (4×3) dimensions was used in the calculations to prevent adsorbate-related lateral interactions, resulting in 12 C atoms per layer. Convergence tests with a variety of MPM grid densities confirmed that sampling only the $\bar{\Gamma}$-point provided an accurate structural and energetic description. Single-molecule structures were calculated in a $10 \times 10 \times 10$ Å^3 cell containing one molecule and again sampling only the Γ-point.

In geometry optimizations, the adsorbed molecule and the four uppermost layers of the slab were allowed to relax until residual forces were smaller than 0.05 eV Å^{-1}. The dynamical properties of the surface reactions were simulated by Born–Oppenheimer molecular dynamics (BO-MD) in a manner identical to that applied recently in our study of ozone reactions on clean and hydrogen-passivated silicon surfaces [27, 28].

To gather information about the electronic structure during the reactions we have also examined the net spin density, $s(\mathbf{r})$,

which is defined as the electron density difference between spin up and spin down electrons ($s(\mathbf{r}) = n_\uparrow(\mathbf{r}) - n_\downarrow(\mathbf{r})$). If integrated over its spatial coordinates, two useful measures of the total spin of the system are obtained: $S = \int s(\mathbf{r}) d\mathbf{r}$ and $\bar{S} = \int |s(\mathbf{r})| d\mathbf{r}$. Only if $\bar{S}$ is zero can one treat the system as spin unpolarized. Both S and $\bar{S}$ may vary during the course of a reaction, since neither is a conserved quantity in an extended system. Therefore, these quantities inform us about spin transitions in the electronic configuration during a simulation and identify the different reaction stages. Then, by visualizing the net spin density $s(\mathbf{r})$, we gain insight into the electronic structure during each reaction stage. In addition, partitioning the electron density allows us to attribute electrons to a specific atom in the system; in the present study, the plane-wave basis set is projected onto a localized basis set to calculate atomic charges and atomic spins by means of Mulliken analysis [29].

3. Static calculations

Before describing our molecular dynamics results, it will be beneficial to revisit some known aspects of the C{001} surface and to consider the adsorption of oxygen thereon.

3.1. The C{001} surface

Of all diamond surfaces, the {001} facet is the most technologically important, justifying its choice for the present study. The (1×1) configuration of C{001} is unstable, however, and readily forms a (2×1) reconstruction in which neighbouring surface atoms move together to form a σ-like dimer bond. Due to the small atomic radius of carbon, the otherwise 'dangling' orbitals remaining after formation of this bond are also able to overlap and form an additional π-like bond. This strained C=C double bond is reflected in the shortened bond length of 1.37 Å (in comparison, the C–C bond length in the bulk lattice is 1.53 Å) and results in the well-known symmetric dimer reconstruction. This provides an interesting point of comparison with our previous work on the oxidation of Si{001} by ozone [27], since the greater atomic radius of silicon results in very little overlap between dangling orbitals; instead, charge transfer between these orbitals leads to an asymmetric dimer, in which the dimer bond itself retains only single bond character. Thus we may anticipate that ozone's reactivity on C{001} will differ from that on Si{001} primarily due to the dimer symmetry and the formal order of the dimer bond.

3.2. Adatom sites for oxygen

To distinguish between the various binding sites for a single O adatom, we adopt a nomenclature based loosely upon the terminology used for functional groups in organic chemistry. Thus, we speak of 'epoxide', 'ether', 'alkoxide' and 'ketone' configurations, as depicted in figure 1. Of these, the most stable is the epoxide structure, with an adsorption heat of 3.59 eV (defined as the heat released when O_3 partially dissociates to leave a single adatom, with triplet O_2 departing into the gas phase). Next in order of stability is the ether structure (2.78 eV), and then the alkoxide and ketone structures
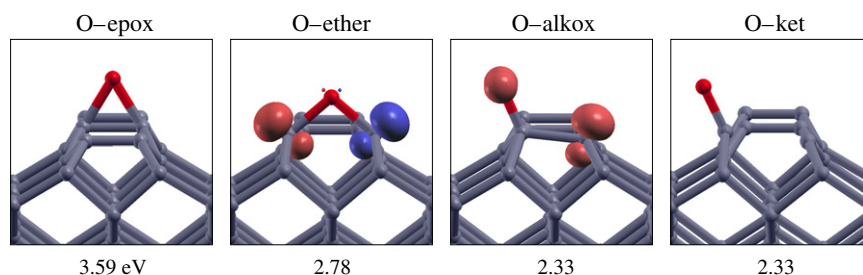
Figure 1. Adsorption structures for a single O adatom on C{001}. Heat of adsorption (eV) is given with respect to the partial dissociation of ozone. In both the ether and the ketone structures, the dimer bond is fully broken.

(both 2.33 eV). Our calculations for these configurations are consistent with prior theoretical studies [30–32], and reveal that the epoxide and ketone structures are non-radical in character, whereas both the ether and the alkoxide structures are biradical. In the ether structure, the two C atoms that originally formed the dimer bond are only three-fold coordinated, and gain spin moments of $\pm 0.72\ \mu_B$. For the alkoxide structure, just one of the C atoms from the dimer is under-coordinated, with a spin moment of $0.74\ \mu_B$, while the O atom attached to the other dimer atom retains a spin moment of $0.48\ \mu_B$ in a p-orbital that lies parallel to the surface and perpendicular to the dimer bond. We may therefore anticipate that both the ether and the alkoxide structures are likely to be highly reactive, existing in our molecular dynamics trajectories only as transient species, while the epoxide and ketone structures are likely to be rather more persistent.

4. Molecular dynamics

We investigate the interaction between O_3 and C{001} by performing first-principles molecular dynamics simulations. To reflect the various degrees of freedom (molecular orientation and position with respect to the surface, its impact velocity, and the surface temperature) a total number of twenty trajectories were simulated.

We find that of these simulated trajectories, only a fraction (six) resulted in a reaction between O_3 and the surface. Thus, in contrast to ozone's high reactivity on the clean silicon surface, where every simulated trajectory was found to lead to a dissociative reaction [27], the diamond surface is clearly considerably less reactive with respect to an incoming ozone molecule. Nevertheless, the reactive trajectories can be classified into two types: one relates to a partial dissociation of O_3 into an O adatom and gas-phase O_2, while the other relates to the complete dissociation of O_3 into three O adatoms.

4.1. Partial dissociation

Here we describe one representative trajectory illustrating partial dissociation, which is the reaction most frequently observed in our simulations. Details differ depending upon the starting configuration of the system, but we aim to focus upon general aspects of the time evolution.

4.1.1. Descriptive sequence of events. In this particular trajectory, the O_3 molecule is initially placed approximately 3.3 Å above the surface, with its plane perpendicular to the surface normal and both terminal atoms at a similar height (figure 2). Terminal O^3 starts directly above the dimer row, while terminal O^2 is located above the trough (as labelled in inset i of the figure). No initial velocities have been assigned to the atoms of the surface slab, while O_3 has an initial velocity of 4 Å ps^{-1} directed towards the surface. The snapshots reveal how ozone, before it is able to dissociate, is steered by the surface into a favourable docking geometry.

Despite all O atoms having initially the same velocity, the molecule soon starts to rotate, as the approaching O atoms each experience a slightly different surface potential. In particular, O^3 is repelled by the proximity of the C dimer, while O^2 is able to travel relatively unperturbed towards the trough. Within 180 fs of the simulation (snapshot ii) the molecule has rotated and the previously perpendicular molecular plane has started to tilt. The O^2–C^1 distance has dropped from 3.44 to 2.50 Å, at an average velocity of 5.2 Å ps^{-1}, which is by 1.2 Å ps^{-1} higher than the initially assigned velocity, revealing the growing attraction between the surface and the incoming molecule.

Gradually, the molecule reaches an orientation favourable for reaction. After 220 fs the distance between O^2 and C^1 begins to decrease dramatically. At 240 fs (snapshot iii) this distance has decreased to 1.71 Å, whereas the length of the dimer bond, C^1–C^2, and ozone's O^2–O^1 bond, are stretched to 1.54 and 1.52 Å, respectively. The O^2–O^1 bond eventually breaks, and the distance between the previous bonding partners continues to increase as the simulation proceeds. The newly formed O_2 molecule desorbs from the surface and has no further influence on the reaction.

The adsorbed O atom accelerates towards its new bonding partner, C^1, while the dimer bond, C^1–C^2, stretches by a significant amount, extending to a temporary maximum of 1.63 Å (at 252 fs). A large part of the heat of adsorption released upon O adsorption leads to sizable C^1–O^2 stretch vibrations, which prove strong enough to even break the C^1–C^2 dimer bond for a time (although the same is not true in *all* our partial dissociation trajectories). Upon adsorption of the O atom, the potential energy drops by approximately 1.4 eV, of which around 0.6 eV is initially transferred into C–O stretch vibrations. At 280 fs (snapshot iv) these O^2–C^1 vibrations go through their second cycle reaching a minimum
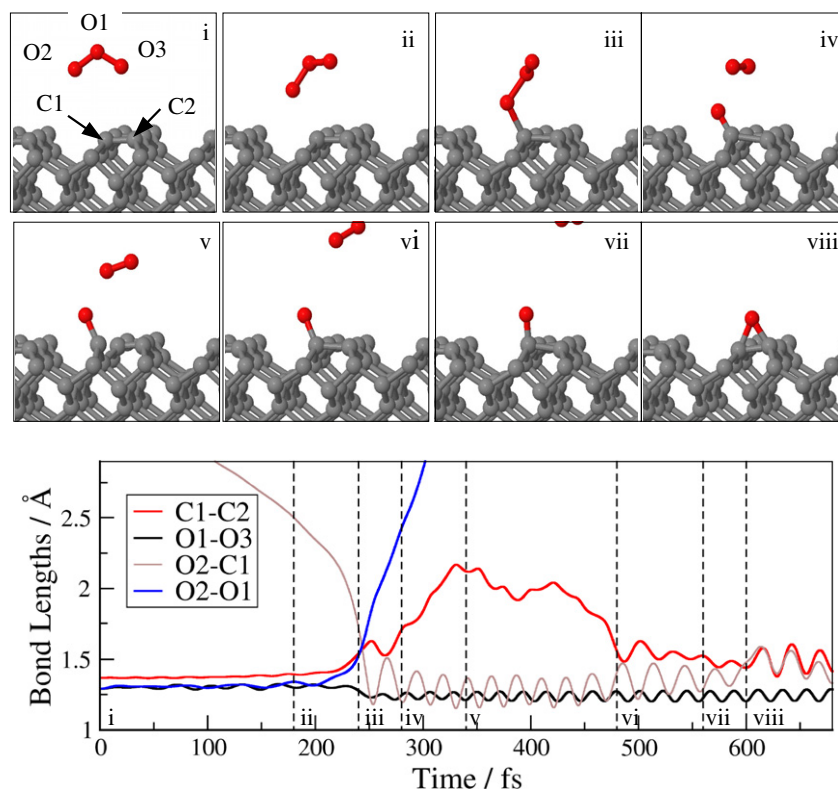
Figure 2. Trajectory resulting in partial dissociation of ozone on C{001}.

distance of 1.19 Å and eventually, at 340 fs (in snapshot v) the C^1–C^2 distance extends to 2.12 Å, which effectively breaks the dimer bond. For an approximate time of 160 fs this dimer bond remains broken, as judged with reference to quasistatic transition state calculations. During this time, the O adatom occupies the ketone structure, where the C=O bond can be classified as a double bond, while the C atom exhibits only two C–C surface bonds (>C=O). In this configuration O^2 and C^1 get closer in distance, so their vibrations shift to a higher frequency. The C=O bond oscillates steadily between minimum and maximum lengths of 1.15 and 1.39 Å, respectively. In comparison, the equilibrium bond length of this structure is 1.25 Å.

However, the cleavage of the C–C bond is only of a temporary nature, and 160 fs later, at 480 fs (snapshot vi), the C^1–C^2 distance has dropped to 1.55 Å. After the re-establishment of the dimer bond, the O^2–C^1 vibrations shift again to a lower frequency, consistent with a C–O single bond, and to higher amplitudes; the structure thus conforms to the alkoxide configuration. In this configuration the bond oscillates between minima and maxima of 1.22 and 1.47 Å, respectively. But this adsorption structure, too, is only a short-lived reaction intermediate and within 120 fs relaxes into the epoxide structure, which is the most stable adsorption site for a single O atom on C{001}. The transition initiates at approximately 560 fs (snapshot vii), when O^2 approaches the under-coordinated C dimer atom, C^2. Finally, at 600 fs (snapshot viii) O^2 forms an additional bond with C^2, and the O^2–C^1 bond stretches slightly. The O adatom occupies this epoxide configuration for the remaining duration of the

simulation (approximately 1 ps). After an initial rise due to the released heat, the O^2–C^1, O^2–C^2 and C^1–C^2 vibrations drop quickly in amplitude as this heat is gradually dissipated into the substrate. The average bond lengths stabilize around 1.40, 1.40 and 1.48 Å, respectively.

4.1.2. Electronic structure during partial dissociation. Figure 3 shows the evolution of the integrated spin density during the trajectory described above (figure 2). In addition, the spin densities of important reaction intermediates are displayed to reveal the electronic configuration underlying the partial dissociation. The electron densities with majority and minority spin will be further referred to as ρ_α and ρ_β, respectively. A Mulliken population analysis was also carried out to relate the spin density to the underlying electron transfer.

The reaction can be classified into five stages, labelled I–V. *Stage I* corresponds to a weak interaction between gas-phase ozone and the diamond surface. The surface donates electron density into the O_3 LUMO, causing a net spin polarization (snapshot i). As one of O_3's terminal O atoms gets closer to a C dimer atom, the adjacent C dimer atom develops an increasing anti-parallel spin density. As the two spin polarizations (i.e. on the molecule and on the surface) are opposite, the integrated spin S eventually drops to zero, although $\bar{S}$ remains large. The presence of this surface spin density can be explained as follows: one of the C dimer atoms interacts with a terminal O atom of the incoming ozone by transferring electrons from the C=C double bond into an emerging C–O bond. As the C=C dimer bond becomes depleted in electrons, the other C dimer atom develops a spin-polarized dangling bond. In the next
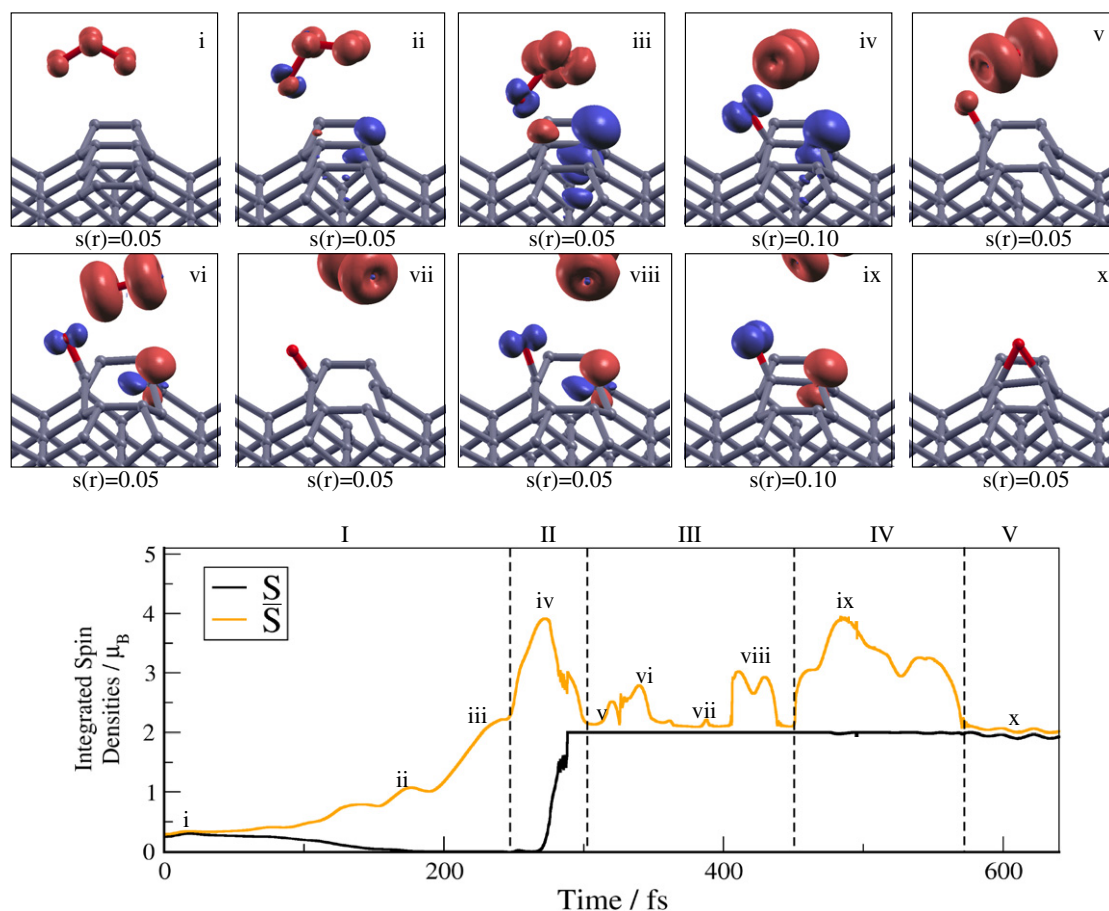
Figure 3. Spin evolution of trajectory showing partial dissociation. Snapshots of the electronic structure are shown with isosurfaces of the net spin densities at either 0.05 or 0.10 μ_B Å^{-3} as marked.

stage, when the C–O bond has formed and the C=C double bond is fully broken, this C dimer atom is left with an unpaired electron, which previously took part in the π bond.

A careful examination of snapshot ii also reveals that the spin density on the terminal O atom exhibits two p-orbitals of opposite polarization. The ρ_α p-orbital aligns with ozone's LUMO, while the ρ_β p-orbital is directed towards the C dimer atom. The ρ_α p-orbital disappears as the ozone reorients. In snapshot iii only the ρ_β p-orbital is present, while the interacting C dimer atom develops a dangling bond of ρ_α polarization. The spin density located on the ozone reveals why this orientation in particular is favourable for dissociation. In this orientation the population of the interacting p-orbital is at its maximum as it is aligned with the dangling bond of the C dimer atom and also with ozone's LUMO.

In *stage II*, ozone has dissociated into gas-phase O_2 and an O atom binding to a C dimer atom (alkoxide structure). In this adsorption site the O adatom exhibits a spin-polarized p-orbital, while the C dimer atom adjacent to the adsorption site exhibits a dangling bond of the same spin polarization. Thus, the freshly formed C–O bond only involves one of the O atom's p-orbitals and the adjacent C dimer atom is lacking a bonding partner for its fourth valence electron. The C–O and C–C dimer bond can also be thought of as single bonds. The gas-phase O_2 molecule relaxes immediately into its triplet configuration and the integrated spin S exhibits an abrupt change from 0 to 2 μ_B.

Stages II–IV can be regarded as short-lived intermediate adsorption structures before, in stage V, the O adatom relaxes into the stable epoxide geometry. In the transition from *stage II* to *stage III*, the O adatom diffuses from the alkoxide (its original adsorption site) into the ketone structure, where the C–C dimer bond is fully broken. Interestingly enough, this structure exhibits two distinct electronic configurations. In snapshots v and vii the under-coordinated C atom does not exhibit any significant spin density, whereas in snapshots vi and viii the two dangling bonds are spin polarized, with one pointing towards its previously bonding C neighbour and the other pointing upwards from the surface. This effect is very likely due to the crossing of two energetically close-lying potential energy surfaces which exhibit different spins. In *stage IV*, the C–C bond has formed again, and the O atom resides again in the alkoxide structure. As the interaction with the gas-phase O_2 is less than before (snapshot iv) the spin density located on the O adatom and the under-coordinated C dimer atom are now of opposite polarization and the adatom's p-orbital is aligned with the dimer row. Finally, in *stage V*, the O atom relaxes into the epoxide structure. The dangling bond of the under-coordinated C dimer atom forms a bond with one of the adatom's p-orbitals and all electrons become paired, so the surface spin density becomes zero everywhere (S and $\bar{S}$ both equal to 2 μ_B, due to triplet gas-phase O_2).
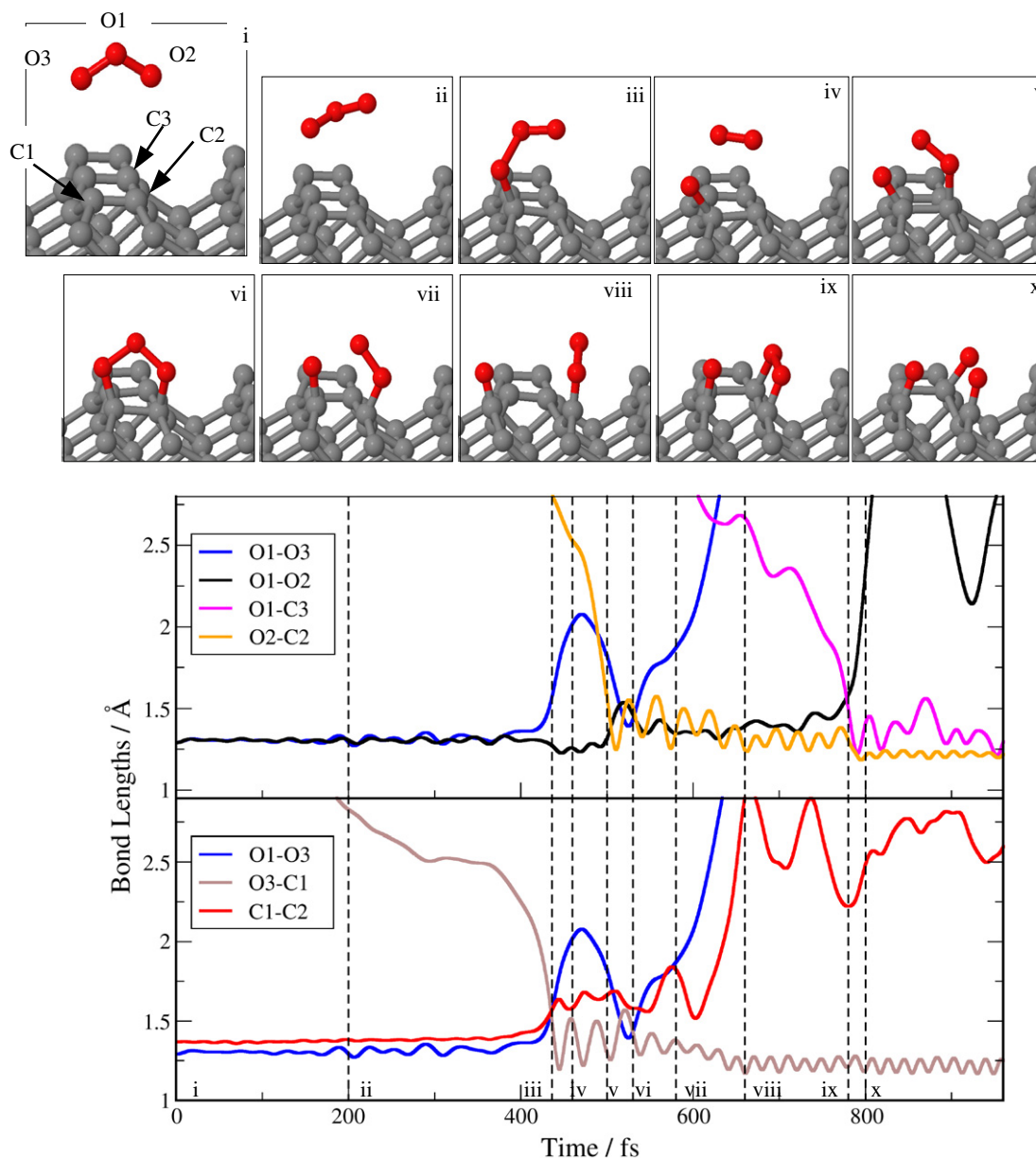
Figure 4. Trajectory resulting in complete dissociation of ozone on C{001}.

4.2. Complete dissociation

In all the reactive trajectories involving partial dissociation, a single O adatom is deposited on the surface, and the resulting O_2 molecule desorbs into the gas phase. In addition to these reactions, however, we also observed other trajectories that resulted in a complete dissociation of ozone, due to the rapid capture of nascent O_2 and its subsequent cleavage on the surface. Again, we focus here upon just one representative trajectory.

4.2.1. Descriptive sequence of events. Trajectories resulting in complete dissociation of O_3 evolve through several reaction intermediates, and are rather more complex than those leading to partial dissociation (figure 4). In this example, the O_3 molecule is initially placed in an orientation similar to that for partial dissociation described above: the molecular plane

is perpendicular to the surface normal, while both its terminal atoms are approximately at the same height above the surface (snapshot i); only the impact parameter varies significantly, with the molecule's centre of mass placed more directly above the dimer bond, rather than one of the dimer atoms. The initial velocity of ozone is 4 Å ps^{-1}, which is directed towards the surface. The simulation reveals that ozone in this orientation experiences a repulsive interaction between its terminal atoms and the carbon dimer underneath. So, instead of directly approaching this dimer, the molecule is deflected from its original path and begins to drift along the dimer row towards a neighbouring dimer. Through the repulsive interaction the molecule rotates into a more parallel orientation with respect to the surface (snapshot ii).

In addition, terminal O^2 moves away from the surface, whereas terminal O^3 gets closer to C^1. At 200 fs the distance between the future bonding partners, O^3–C^1, has dropped to

2.82 Å, and continues to decrease. Between 300 and 370 fs, however, this distance stays temporarily at a plateau of 2.50 Å, until the molecule reaches a position directly above the dimer. Then, after a further 40 fs the dissociation is initiated by a sudden drop in the O^3–C^1 distance. Simultaneously, the O^3–C^1 surface bond forms while ozone's O^1–O^3 bond breaks. At 440 fs (snapshot iii) the decreasing O^3–C^1 distance eventually crosses the increasing intramolecular O^1–O^3 and dimer bond C^1-C^2. Eventually O^3–C^1 reaches a minimum distance of 1.20 Å, while C^1-C^2 reaches its first maximum of 1.63 Å at approximately 450 fs. The average O^1–O^2 bond length of the freshly formed O_2 drops from 1.30 to 1.24 Å. Molecular oxygen drifts away from its previous O bonding partner, but approaches the adjacent dimer atom, C^2. Instead of desorbing, as occurred in the previous trajectory, O_2 is attracted towards the under-coordinated C^2, where it reacts to form a single bond, as visualized at 500 fs (snapshot v). Within a short time, the dangling atom, O^1, combines with O^3 to form an adsorbed species, which can be seen at 530 fs (snapshot vi). Based upon the nomenclature of organic chemistry, this five-membered ring, with three contiguous oxygen atoms and two contiguous carbon atoms, may be described as a 'molozonide'.

Molozonides are typically formed during the ozonolysis of alkenes, where a C=C double bond is attacked by ozone to form a characteristic five-membered ring of just the kind seen here. The molozonide structure in organic systems is usually only a short-lived intermediate, however, which readily cleaves at the C–C bond, and at one of the O–O bonds, prior to rearrangement into a different five-membered ring with only a single O–O bond and four alternating C–O bonds, known as an 'ozonide'. In the present simulations also, the molozonide lifetime is very short indeed, cleaving across O–O and C–C bonds within 40 fs (snapshot vii). For steric reasons, rearrangement into an ozonide analogue is not possible at the surface. Instead, the dangling O atom (i.e. the untethered end of the O_2 moiety) is eventually attracted by a C atom from an adjacent dimer along the same row (snapshot viii). For a short while, the O_2 moiety remains intact, bridging between neighbouring dimers (snapshot ix), but soon it too dissociates leaving three O adatoms on the surface. Of these, two exhibit ketone structures involving the atoms of the original dimer, while the third is in an alkoxide configuration on the adjacent dimer (snapshot x). The alkoxide shows initially strong C–O vibrations, reaching elongations of up to 1.56 Å, but nevertheless persists for the remaining duration of the simulation (lifetime greater than 600 fs); we do expect, however, that a transition to the epoxide structure should eventually occur in due course. The C=O oscillations of the ketone groups, meanwhile, occur in our simulations at a frequency of 1750 ± 30 cm^{-1}, in excellent agreement with surface ketone modes observed in experiment in the vicinity of 1730 cm^{-1} [33, 34].

4.2.2. Electronic structure during complete dissociation. Figure 5 shows the evolution of the integrated spin density during the trajectory described above (figure 4). In addition, the spin densities of important reaction intermediates are displayed to reveal the electronic configuration underlying the

complete dissociation. The reaction can be classified into six stages, labelled I–VI.

In *stage I*, gas-phase ozone approaches the diamond surface and initially there is only a weak interaction through charge transfer. While the molecule remains some distance above the surface, spin densities are localized on the incoming molecule in regions corresponding to its LUMO (snapshot i). As ozone gets progressively closer, however, spin densities of opposite polarization emerge on one of the C dimer atoms and in ozone's HOMO (snapshot ii). The total spin S drops to zero, but no reaction between ozone and the dimer is observed. In this orientation, ozone's HOMO overlaps with the C dangling bond, whereas the partially occupied LUMO cannot interact strongly due to symmetry considerations. This orientation is therefore not favourable for dissociation.

Instead, ozone reorients so that the LUMO is able to overlap with the C dangling bond, allowing dissociation to take place. The integrated spin S remains zero, but the local distribution of spin density changes, reflected in $s(\mathbf{r})$ and $\bar{S}$. The p-orbitals that previously constituted the LUMO now no longer share the same spin polarization, suggesting that significant rehybridization is underway within the molecule. In particular, the p-orbital of the terminal atom closest to C^1 exhibits opposite polarization to the p-orbitals of the other O atoms. In addition, spin densities of opposite polarization are located on the C^2 atom (snapshot iii), indicating that electron transfer into the nascent C–O bond depletes the C=C double bond and leaves C^2 with an unpaired electron. As the initial partial dissociation takes place, a spin density emerges on C^1, which is of opposite polarity to the binding O atom and to C^2 (snapshot iv).

Stage II characterizes the phase directly after the initial partial dissociation, when atomic O is bound to a dimer atom and the newly formed O_2 is temporarily free from covalent interaction with the surface (snapshot vi). The spin density located on O_2 shows the typical triplet configuration expected in the gas phase, whereas the surface exhibits spin densities localized on the O adatom and on C^2, which relate to one of the O p-orbitals and the C dangling bond. These densities are of opposite polarization, so the integrated spin S is zero, while $\bar{S}$ reaches its maximum value of 3 μ_B.

Until this point, the spin evolution of this trajectory is almost identical to that observed during partial dissociation (figure 3). In *stage III*, however, the O_2 molecule binds to the surface and differences emerge. Electron density is transferred from the C^2 dangling bond into the overlapping π-orbital of the molecule, with a concomitant drop in the spin density; only the π-orbital parallel to the surface remains spin polarized (snapshot vii).

In *stage IV*, the molozonide forms, as the singly occupied orbitals of the O adatom and the adsorbed O_2 form a bond (snapshot viii). While the molozonide persists, the integrated spins S and $\bar{S}$ are both zero, but as noted above, this species has only a very short lifetime. Indeed, the entire progression through *stages II–IV* is complete in little more than 100 fs. Subsequently, in *stage V*, the molozonide dissociates again into two separate surface bound species of atomic O and molecular O_2, and the C–C dimer bond breaks. In this stage, several
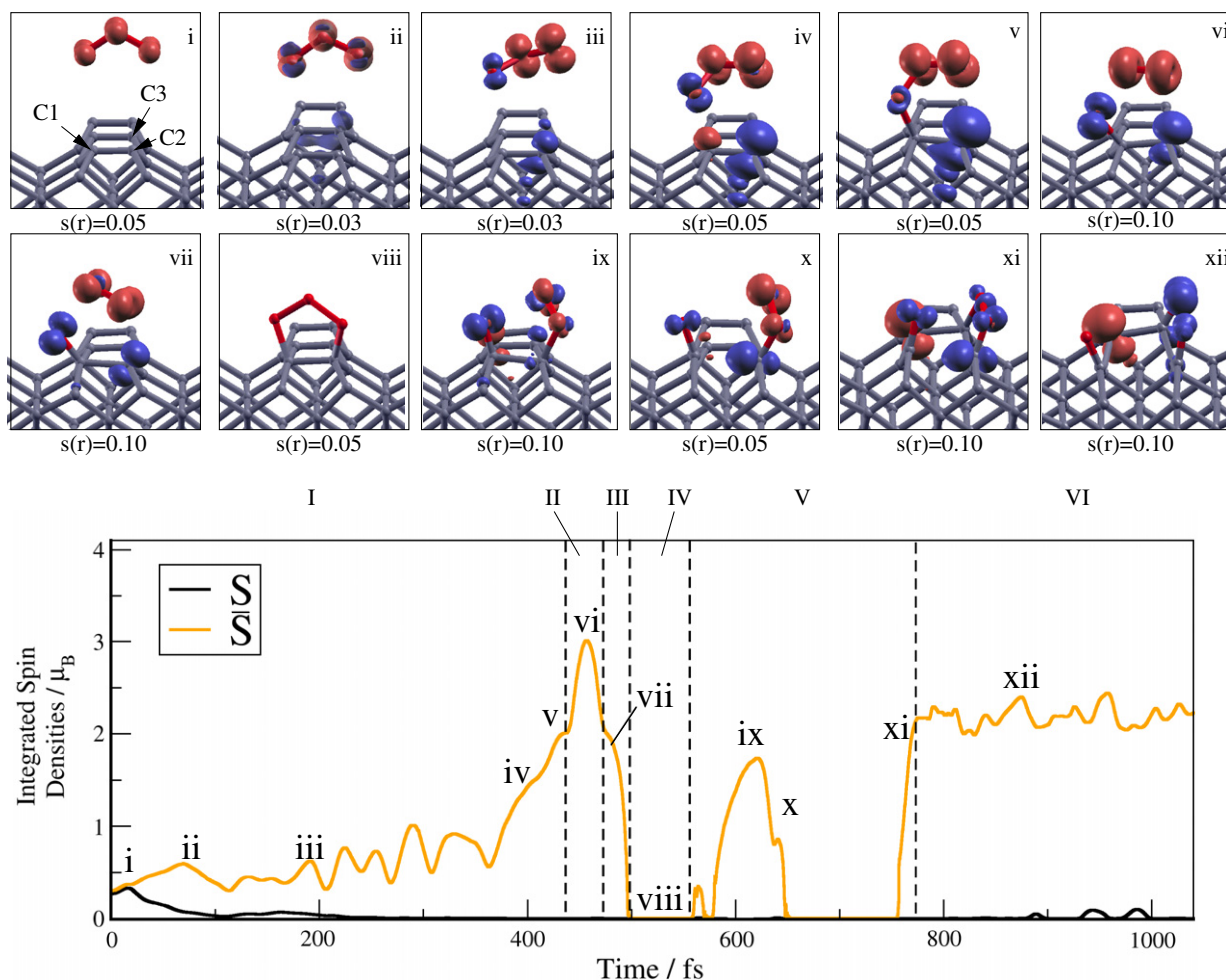
Figure 5. Spin evolution of trajectory showing complete dissociation. Snapshots of the electronic structure are shown with isosurfaces of the net spin densities at 0.03, 0.05 or 0.10 μ_B Å^{-3} as marked.

spin configurations appear. In snapshot ix the C–C bond is still intact and the O_2 moiety exhibits two spin-polarized π-orbitals of opposite polarization. Then the C–C dimer breaks, one of C^2's sp^3 hybridized orbitals becomes spin polarized and only one of O_2's π-orbitals is spin polarized (snapshot x). Although the C–C dimer bond is now permanently broken, the spin densities disappear for a period of 130 fs, between 650 and 780 fs into the simulation. During this period, the O_2 moiety is bound through one end to the C dimer atom, while the isolated O adatom is bound to the other C^1 dimer atom in the ketone structure. In this configuration, the spin-polarization $\bar{S}$ is zero, suggesting that the dangling O_2 is able to saturate both unpaired valence electrons of the C^2 dimer atom.

In the final phase, *stage VI*, the dangling O_2 binds to a neighbouring dimer atom along the dimer row and dissociates into two O adatoms. Snapshot xi highlights how O_2 bridges to the nearby dimer atom, C^3, revealing that spin densities of the same polarization appear on C^2 and the O atoms. The two p-orbitals localized on these adatoms are not parallel with respect to each other, indicating that the molecular π-orbital is splitting into its constituent atomic p-orbitals. In addition, a spin density of opposite polarization appears on the dimer bonding partner of C^3, due to C^3–O^1 bond formation converting a double (C=C) into a single (C–C) dimer bond and implying a dangling

bond at the other end of the dimer. In snapshot xii, O_2 has dissociated, leaving three individual O adatoms. Two of these are located on the same dimer, occupying the ketone structure, while the third binds in the alkoxide structure. The ketones are spin unpolarized, while the alkoxide has polarization similar to that seen for the same structure during the partial dissociation trajectory described previously.

5. Conclusion

Our simulations reveal that ozone readily oxidizes the clean diamond surface[2], albeit the reactivity is somewhat lower than that found on the clean silicon surface [27]. On Si{001}, we noted that partial or complete dissociation was dependent on which of the two inequivalent dimer atoms was attacked by

---

[2] We note in passing that our MD simulations for ozone interaction with partially oxidized or hydrogen-passivated diamond surfaces reveal significantly reduced reactivity compared to the clean surface. We should, however, also point out that the adiabatic approximation is suspect in the case of hydrogen-terminated diamond. This is because that surface has a negative electron affinity, so that significant charge transfer between surface and molecule occurs even at large distances. In reality, low tunnelling rates should prevent this electron transfer until the molecule is close to the surface, but the adiabatic approximation allows it to occur instantaneously at any distance.

ozone. Here, we find that partial dissociation occurs on C{001} when the incoming molecule interacts first with either one of the two equivalent dimer atoms, so long as the resulting oxygen molecule desorbs from the surface; the adatom initially adopts a biradical alkoxide structure, before shifting to a non-radical epoxide configuration. In contrast, when partial dissociation yields an oxygen molecule sufficiently close to the carbon radical centre of the alkoxide, the system forms a transient molozonide, which subsequently cleaves in the manner familiar from organic chemistry to yield two surface ketones and an alkoxide; the latter is expected eventually to revert to an epoxide. The {001} surface of diamond is thus distinguished from that of silicon by the symmetry of its dimers, and the fact that their reactivity towards ozone is reminiscent of the ozonolysis of alkenes. The analogy with organic chemistry is strikingly apposite, and we believe may be extendable (with care) to other surface reactions of diamond.

Acknowledgments

References

[1] Kalish R 2007 Diamond as a unique high-tech electronic material: difficulties and prospects *J. Phys. D: Appl. Phys.* **40** 6467–78

[2] Wort C J H and Balmer R S 2008 Diamond as an electronic material *Mater. Today* **11** 22–8

[3] Nebel C E and Ristein J 2004 *Thin-film diamond II. Semiconductors and Semimetals* 1st edn (Amsterdam: Elsevier)

[4] Ristein J 2006 Surface science of diamond: familiar and amazing *Surf. Sci.* **600** 3677–89

[5] Chakrapani V, Angus J C, Anderson A B, Wolter S D, Stoner B R and Sumanasekera G U 2007 Charge transfer equilibria between diamond and an aqueous oxygen electrochemical redox couple *Science* **318** 1424–30

[6] Nebel C E 2007 Surface-conducting diamond *Science* **318** 1391–2

[7] Ristein J 2006 Surface transfer doping of semiconductors *Science* **313** 1057–8

[8] Zheng X M and Smith P V 1992 The stable configurations for oxygen chemisorption on the diamond (100) and (111) surfaces *Surf. Sci.* **262** 219–34

[9] Skokov S, Weiner B and Frenklach M 1994 Molecular-dynamics study of oxygenated (100) diamond surfaces *Phys. Rev. B* **49** 11374

[10] Wang Y M, Wong K W, Lee S T, Nishitani-Gamo M, Sakaguchi I, Loh K P and Ando T 2000 Recent studies on diamond surfaces *Diamond Relat. Mater.* **9** 1582–90

[11] John P, Polwart N, Troupe C E and Wilson J I B 2002 The oxidation of (100) textured diamond *Diamond Relat. Mater.* **11** 861–6

[12] Lee J-K, Anderson M W, Gray F A, John P, Lee J-Y, Baik Y-J and Eun K Y 2004 Oxidation of cvd diamond powders *Diamond Relat. Mater.* **13** 1070–4

[13] de Theije F K, Roy O, van der Laag N J and van Enckevort W J P 2000 Oxidative etching of diamond *Diamond Relat. Mater.* **9** 929–34

[14] deTheije F K, van der Laag N J, Plomp M and van Enckevort W J P 2000 A surface topographic investigation of {001} diamond surfaces etched in oxygen *Phil. Mag.* A **80** 725–45

[15] Alvarez J, Kleider J P, Snidero E, Bergonzo P, Tromson D and Mer C 2004 On the metastability of the surface conductivity in hydrogen-terminated polycrystalline cvd diamond *Diamond Relat. Mater.* **13** 751–4

[16] Riedel M, Ristein J and Ley L 2004 The impact of ozone on the surface conductivity of single crystal diamond *Diamond Relat. Mater.* **13** 746–50

[17] Riedel M, Ristein J and Ley L 2004 Recovery of surface conductivity of H-terminated diamond after thermal annealing in vacuum *Phys. Rev. B* **69** 125338

[18] Petrini D and Larsson K 2007 Electron transfer from a diamond (100) surface to an atmospheric water adlayer: a quantum mechanical study *J. Phys. Chem.* C **111** 13804–12

[19] Sakai T, Song K-S, Kanazawa H, Nakamura Y, Umezawa H, Tachiki M and Kawarada H 2003 Ozone-treated channel diamond field-effect transistors *Diamond Relat. Mater.* **12** 1971–5

[20] Chong K F, Loh K P, Vedula S R K, Lim C T, Sternschulte H, Steinmuller D, Sheu F-S and Zhong Y L 2007 Cell adhesion properties on photochemically functionalized diamond *Langmuir* **23** 5615–21

[21] Petrov I, Shenderova O, Grishko V, Grichko V, Tyler T, Cunningham G and McGuire G 2007 Detonation nanodiamonds simultaneously purified and modified by gas treatment *Diamond Relat. Mater.* **16** 2098–103

[22] Maranzana A, Serra G, Giordana A, Tonachini G, Barco G and Causa M 2005 Ozone interaction with polycyclic aromatic hydrocarbons and soot in atmospheric processes: theoretical density functional study by molecular and periodic methodologies *J. Phys. Chem.* A **109** 10929–39

[23] Segall M D, Lindan P J D, Probert M J, Pickard C J, Hasnip P J, Clark S J and Payne M C 2002 First-principles simulation: ideas, illustrations and the CASTEP code *J. Phys.: Condens. Matter* **14** 2717–44

[24] Vanderbilt D 1990 Soft self-consistent pseudopotentials in a generalized eigenvalue formalism *Phys. Rev. B* **41** 7892

[25] Perdew J P, Chevary J A, Vosko S H, Jackson K A, Pederson M R, Singh D J and Fiolhais C 1992 Atoms, molecules, solids, and surfaces: applications of the generalized gradient approximation for exchange and correlation *Phys. Rev. B* **46** 6671–87

[26] Monkhorst H J and Pack J D 1976 Special points for brillouin-zone integrations *Phys. Rev. B* **13** 5188–92

[27] Fink C K and Jenkins S J 2008 First-principles molecular dynamics of the initial oxidation of Si{001} by ozone *Phys. Rev. B* **78** 195407–10

[28] Fink C K and Jenkins S J 2008 Radical-mediated adsorption: ozone oxidation of passivated silicon *Surf. Sci.* **602** L100–3

[29] Segall M D, Shah R, Pickard C J and Payne M C 1996 Population analysis of plane-wave electronic structure calculations of bulk materials *Phys. Rev. B* **54** 16317

[30] Rutter M J and Robertson J 1998 *Ab initio* calculation of electron affinities of diamond surfaces *Phys. Rev. B* **57** 9241

[31] Sque S J, Jones R and Briddon P R 2006 Structure, electronics, and interaction of hydrogen and oxygen on diamond surfaces *Phys. Rev. B* **73** 085313

[32] Petrini D and Larsson K 2007 A theoretical study of the energetic stability and geometry of hydrogen- and oxygen-terminated diamond (100) surfaces *J. Phys. Chem.* C **111** 795–801

[33] Hossain M Z, Kubo T, Aruga T, Takagi N, Tsuno T, Fujimori N and Nishijima M 1999 Chemisorbed states of atomic oxygen and its replacement by atomic hydrogen on the diamond (100)-(2 × 1) surface *Surf. Sci.* **436** 63–71

[34] John P, Polwart N, Troupe C E and Wilson J I B 2003 The oxidation of diamond: the geometry and stretching frequency of carbonyl on the (100) surface *J. Am. Chem. Soc.* **125** 6600–1